Retrieval of snow albedo and total ozone column from single-view MSI/S-2 spectral reflectance measurements over Antarctica

A. Kokhanovsky (1), S. Gascoin (2), L. Arnaud (3) , G. Picard (3)

(1) Telespazio Belgium, Bratustarsse 7, 64289 Darmstadt, Germany

(2) CESBIO, Université de Toulouse, CNES/CNRS/INRA/IRD/UPS, 31400 Toulouse, France

(3) Uniersity Grenoble Alpes, CNRS, Institut des Géosciences de l'Environnement (IGE), UMR 5001, 38041 Grenoble, France

Abstract

We have proposed a simple algorithm to retrieve the total ozone column and snow properties (spectral albedo and effective light absorption path) using the high spatial resolution *single – view* MSI/S-2 measurements over Antarctica. Therefore, multiple observations of the same ground pixel from different directions as used, e.g., in the MODIS snow albedo retrieval algorithm (Schaaf et al., 2002) are not needed.

Keywords : snow, total zone, Antarctica, radiative transfer, light scattering,, optical snow grain sizing

 doi:10.20944/preprints202109.0388.v1

1. Introduction

Sentinel-2 (S-2) is an Earth observation mission from the Copernicus Programme that systematically acquires optical imagery at high spatial resolution (10 m to 60 m) over land and coastal waters. The mission is a constellation with two twin satellites, S-2A and S-2B. The satellites have been launched on June 23, 2015 and March 7, 2017, respectively. It is planned that S–2C and S–2D will be launched during next 10 years. The S-2 mission is equipped with the Multi-Spectral Instrument (MSI), which uses a push-broom concept and its design has been driven by the large (290km) swath and high (10-60m) spatial resolution requirements. Revisiting is 5 days per month on average under the same viewing angles close to the nadir direction. MSI operates in the spectral range 0.44-2.2μm. The instrument has already been used for numerous applications including studies of lake ecological quality (Free et al., 2020), winter wheat (Zhang et al., 2019) and seasonal agriculture land use (Debella - Gilo, 2021) mapping, estimation of fractional vegetation cover (Wang et al., 2018), etc. (see, e.g., https://www.mdpi.com/journal/remotesensing/special_issues/sentinel2_sa).

Gascoin et al. (2019, 2020) have used MSI/S-2 data for the estimation of the fractional snow cover (FSC) at 20m resolution in open terrain. However, climatic effects of snow cover depend not only on its extent (Peng et al., 2021), but also on its spectral albedo, which plays an important role in the modification of the backscattered solar energy on local and global scales (Flanner et al., 2007; 2021). Snow albedo products are currently available at moderate resolution (i. e., 300m from Ocean and Land Colour Imager (OLCI) (Kokhanovsky et al., 2019, 2020), 500m from MODerate Imaging Spectrometer (MODIS) (Schaaf et al., 2002; Hall et al, 2002) and Sea and Land Surface Temperature Radiometer (SLSTR) (Mei et al., 2021a,b), and 1km from Second Generation Global Imager (SGLI) (Chen et al., 2021)). However, they do not allow capturing the fine details of spatial variability of the snow surface properties (Schweizer et al., 2008). The technique presented here provides snow albedo product on the scale of 10-20m and makes it possible to derive and validate subpixel snow cover products as obtained, e.g., from MODIS measurements (Kaufman et al., 2002 ; Painter et al., 2009).

The task of this paper is to derive the spectral snow albedo using MSI/S-2A (B) 10-60m spatial resolution reflectance data. The spatial resolution of the product depends on the spectral channels used. In addition, the algorithm to determine the total ozone column (TOC) over snow fields using MSI/S-2 is proposed. The retrieval algorithm is described in the next section. We also present the validation of the algorithm using ground – based snow spectral albedo and

Preprints (www.preprints.org) | NOT PEER-REVIEWED | Posted: 22 September 2021 doi:10.20944/preprints202109.0388.v1

TOC measurements performed at Dome C (75°05′59″S, 123°19′56″E, 3233m above sea level) in Antarctica.

2. The determination of the total ozone and spectral snow albedo using MSI measurements

This work is aimed at the retrievals of total ozone column and snow properties from MSI measurements over Antarctica. The atmospheric light scattering effects are rather weak (Six et al., 2005; Tomasi and Petkov, 2015) in Antarctica for the MSI channels (see Table 1). Also the concentration of light absorbing impurities in most Antarctic snow is very low (Grenfell et al., 1994; Kang et al., 2020) and can be neglected in a first iteration. We shall use the following approximation for the spectral top-of-atmosphere reflectance:

$$\Re = T_g R, \tag{1}$$

where T_g is the atmospheric gaseous transmittance, R is the underlying surface – atmosphere reflectance under assumption that there are no absorbing gases in the atmosphere. Ignoring weak atmospheric light scattering effects at the MSI channels, we can write for highly reflective clean Antarctic surfaces (Kokhanovsky et al., 2020a):

$$R = R_0 \exp\left\{-\sqrt{\alpha L}\right\}, \tag{2}$$

where $\alpha = \frac{4\pi\chi}{\lambda}$ is the bulk absorption coefficient of ice, χ is the imaginary part of ice refractive index and λ is the wavelength. Here, R_0 is the snow reflectance in the absence of absorption and L is the effective light absorption path (ELAP). In the case of dirty snow, Eq. (2) must be modified to account for the snow pollutants as discussed by Kokhanovsky et al. (2021).

The task of this work is to retrieve the spectral snow albedo and total ozone concentration using MSI measurements in the spectral range 443-865nm, where the accuracy of Eq. (2) is higher as compared to the case of short-wave infrared wavelengths (Kokhanovsky et al., 2019). Also the influence of all atmospheric gases on the value of transmittance T_g (except ozone) can be neglected in this spectral interval (Kokhanovsky et al., 2020b). This is especially valid in central Antarctica, where the atmosphere is thin and air is dry.

Preprints (www.preprints.org) | NOT PEER-REVIEWED | Posted: 22 September 2021 doi:10.20944/preprints202109.0388.v1

We shall use the following approximation for the atmospheric ozone transmittance (Kokhanovsky et al, 2020a):

$$T_g(\lambda) = \exp\{-KC_{abs}(\lambda)\}, \quad (3)$$

where $K=mN$, m is the airmass factor (AMF) depending on several parameters including the cosine of the solar zenith angle (SZA) ξ and the cosine of the viewing zenith angle η, N is the total ozone column and $C_{abs}(\lambda)$ is the ozone absorption cross section. The dependence of $C_{abs}(\lambda)$ on temperature and pressure is weak in the spectral range under study (Gorshelev et al., 2014). Therefore, it is not accounted for.

Summing up, the spectral MSI reflectance over pure snow fields under clear sky is modelled as

$$\Re(\lambda) = R_a \exp\left\{-KC_{abs}(\lambda) - \sqrt{L\alpha(\lambda)}\right\}, \quad (4)$$

where we have assumed that light reflectance by snow at absence of absorbers R_0 can be substituted by the MSI measurements at band 1 (R_a). The weak influences of atmospheric scattering effects on the value of MSI spectral reflectance at 442.7nm can be accounted, if needed, using either exact radiative transfer calculations for a given atmospheric model or various approximations (Kokhanovsky, 2020c). These effects are ignored in this work.

Our simplified model of the MSI spectral reflectance in the visible and near infrared given by Eq. (4) makes it possible to determine two unknown constants (K, L) from Eq. (4) analytically. Namely, it follows:

$$K = \frac{\ln(R_b / R_a) + \sqrt{\alpha_b L}}{C_{abs,b}}, \; L = \frac{\ln^2(R_c / R_a)}{\alpha_c}, \quad (5)$$

where indices signify the spectral channels ($\lambda_a, \lambda_b, \lambda_c$). The wavelength λ_b corresponds to the maximal ozone absorption in the MSI spectra (559.8nm). It has the spatial resolution 10m. The channels (λ_a, λ_c) are used for the determination of the effective light absorption path in snowpack. We shall use the following wavelengths for MSI/S-2A (and similar channels for S-2B) in this work: λ_a=442.7nm and λ_c=864.7nm. They have the same bandwidths (21nm) but different spatial resolutions (60m for the channel located at λ_a and 20m for the channel located at λ_c). The channel located at λ_c=864.7nm corresponds to the maximal ice absorption in the

Preprints (www.preprints.org) | NOT PEER-REVIEWED | Posted: 22 September 2021 doi:10.20944/preprints202109.0388.v1

MSI spectra in the range 443-865nm (with negligible ozone absorption effects). The channel located at λ_a =442.7nm corresponds to the minimal effects of the ice and ozone absorption in the MSI visible range. The use of channels with different spatial resolutions is justified, if snow reflectance in channel 1 (**8A**) weakly change on the scale 10-60(**20**)m, which is true for Antarctic surfaces on average.

Table 1. The specification of the MSI spectral channels. Band 9 is useful for the total water vapor column estimation and band 10 is used for the detection of Cirrus clouds. Bands 1 – 8 are used in atmospheric correction procedures. Bands 11 and 12 can be used to distinguish cloud and clear sky snow fields.

	Sentinel-2A		Sentinel-2B		
Sentinel-2 bands	Central wavelength (nm)	Bandwidth (nm)	Central wavelength (nm)	Bandwidth (nm)	Spatial resolution (m)
Band 1	442.7	21	442.2	21	60
Band 2	492.4	66	492.1	66	10
Band 3	559.8	36	559.0	36	10
Band 4	664.6	31	664.9	31	10
Band 5	704.1	15	703.8	16	20
Band 6	740.5	15	739.1	15	20
Band 7	782.8	20	779.7	20	20
Band 8	832.8	106	832.9	106	10
Band 8A	864.7	21	864.0	22	20
Band 9	945.1	20	943.2	21	60
Band 10	1373.5	31	1376.9	30	60
Band 11	1613.7	91	1610.4	94	20
Band 12	2202.4	175	2185.7	185	20

The fit of the MSI spectral reflectance measured in the vicinity of the Dome C in Antarctica using Eqs. (4), (5) is given in Fig.1. We extracted reflectances from MSI/Sentinel-2 level 1C products at the nearest pixel of the measurement site using Google Earth Engine (Gorelick et al., 2017). The solar and sensor geometry parameters for each spectral band were obtained from

Preprints (www.preprints.org) | NOT PEER-REVIEWED | Posted: 22 September 2021 doi:10.20944/preprints202109.0388.v1

the product metadata. The spectral range 400-1050nm is shown in Fig.1. The calculations using Eq. (4) have been performed with the spectral resolution 1nm. The spectral imaginary part of ice refractive index as suggested by Picard et al. (2016a) has been used (at the wavelengths below 600nm). For the larger wavelengths, Warren and Brandt (2008) data for the function $\chi(\lambda)$ has been used. The spectral absorption cross section of ozone $C_{abs}(\lambda)$ measured by Gorshelev et al. at 203K (2012) has been used. The corresponding parameters appearing in Eq. (5) are given in Table 2. The linear interpolation of tabular spectra $C_{abs}(\lambda)$ and $\chi(\lambda)$ on the 1nm grid in the spectral interval 400-1050nm has been applied.

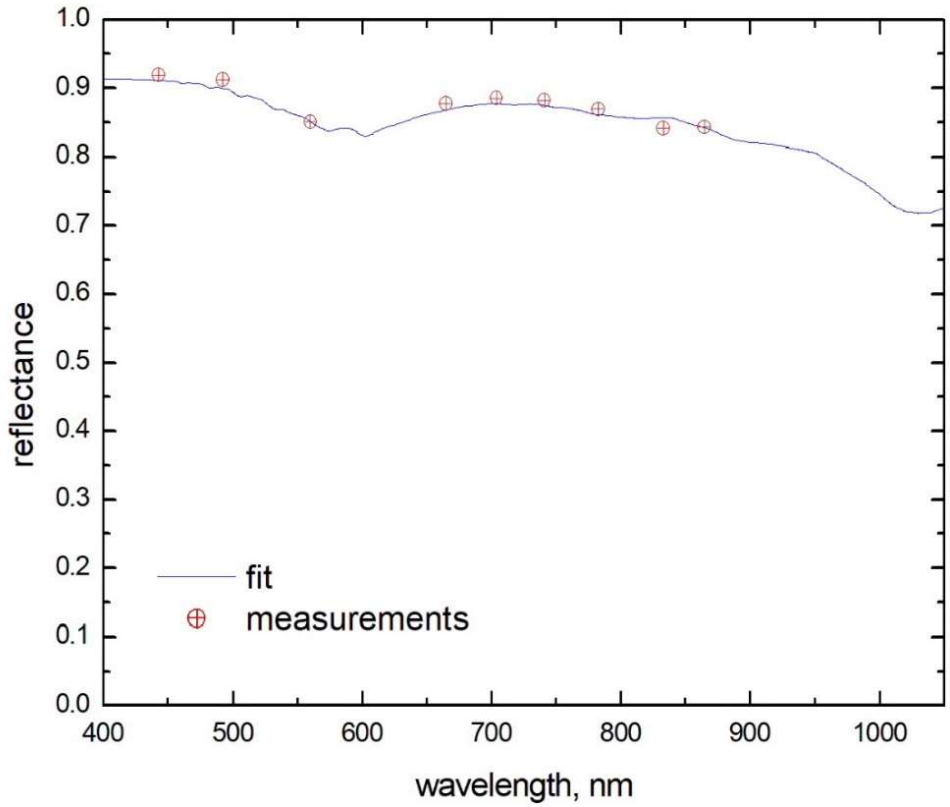

Fig.1. The fit of MSI spectral reflectance over Dome C (Antarctica) (see Eq. (4)). The measurements have been performed on November 3, 2020 during the ozone hole occurrence (Kokhanovsky et al., 2021b).

Table 2. The parameters used in Eq. (5)

Preprints (www.preprints.org) | NOT PEER-REVIEWED | Posted: 22 September 2021 doi:10.20944/preprints202109.0388.v1

$\alpha_b,\ cm^{-1}$	α_c, cm^{-1}	$C_{abs,b},\ cm^2 / molecule$
7.48×10^{-4}	3.49×10^{-2}	3.87×10^{-21}

The retrieved values of the parameters given in Eq. (4) for the case shown in Fig. 1 are: $K=1.66\times10^{19}\ cm^2 / molecule$ and $L=2.13mm.$ They have been derived using Eq. (5) and data given in Table 2.

The total ozone column can be derived from the value of K as follows: $N=K/m$. Assuming that m is given by the geometrical approximation ($m=\frac{1}{\xi}+\frac{1}{\eta}$), one derives for the value of TOC for the case shown in Fig.1: $N=4.8458\times10^{18}\ molecule / cm^2$ or N=180.4DU, where we used the conversion factor $\kappa=3.722\times10^{-17}\ DU\times\ cm^2 / molecule$ to derive the value of N in Dobson Units (DU). The ground SAOZ (Système d'Analyse par Observations Zénithales) TOC measurements (Pommereau and Goutail, 1988; Sarkissian et al., 1997) at the Dome C site give the value of TOC equal to 158 and 180 DU in morning and evening, respectively, which is close to the TOC derived using MSI/S-2 measurements.

The value of L can be used to derive the effective absorption length ℓ, which determines the snow spherical albedo (Kokhanovsky et al., 2019):

$$r=\exp\left\{-\sqrt{\alpha\ell}\right\}. \tag{6}$$

Namely, it follows (Kokhanovsky et al., 2019):

$$\ell=\frac{R_a^2}{u^2(\xi)u^2(\eta)}L, \tag{7}$$

where (Kokhanovsky et al., 2021):

$$u(\mu)=\frac{3}{5}\xi+\frac{1+\sqrt{\xi}}{3}. \tag{8}$$

The function $u(\xi)$ describes angular distribution of light escaping from semi-infinite nonabsorbing turbid media with light sources placed at infinity. Taking into account that R_a = 0.92, ξ =0.41, η =1, and L=2.13mm for the case shown in Fig.1, it follows that $\ell=1.79mm$. This makes it possible to derive both spectral spherical r (see Eq. (6)) and plane ($r_p=r^{u(\mu)}$) albedo (Kokhanovsky et al., 2019). Moreover, the snow effective diameter can be derived:

Preprints (www.preprints.org) | NOT PEER-REVIEWED | Posted: 22 September 2021 doi:10.20944/preprints202109.0388.v1

$d_{ef} = \ell / \sigma$, where σ is the shape factor, which depends on the assumed shape of snow grains. We shall use the value of σ=16 as suggested by Kokhanovsky et al. (2019). Therefore, it follows for the case shown in Fig.1: d_{ef}=0.11mm, which is a reasonable estimation for the snow surface at Dome C (Grenfell et al., 1994; Flanner et al., 2021). In particular, Grenfell et al. (1994) has found the values of d_{ef}=0.1mm in the first 5mm of snow at South Pole (January 23, 1986). The value of d_{ef} was two times smaller at the same location immediately after the snowfall (Grenfell et al., 1994).

The total ozone column over Dome C retrieved using the technique described above for November – December, 2020 is shown in Fig.2 (MSI). The cloudy scenes have been removed using MSI measurements at 2.2 μm with the assumption that clouds have higher reflectance as compared to snow at this channel due to smaller size of crystals in clouds as compared to snow on the surface. The threshold value of R(2.2 μm)=0.2 has been used. The air mass factor has been calculated as (Iqbal, 1983; Savastiouk and McErloy, 2004)

$$m = \frac{1+s}{\sqrt{2s+\xi^2}} + \frac{1+s}{\sqrt{2s+\eta^2}}, \quad (9)$$

where $s = \frac{h}{R}, h = 0.26 - 0.1L$, L is the latitude in degrees (the negative number in the southern hemisphere), R is the radius of the Earth, h is the height of the ozone layer in km. Eq. (9) coincides with the geometrical AMF at s=0. We also show the TOC derived from other satellite/ground observations (see Table 3 and Kokhanovsky et al. (2021b) for details on various satellite measurements) and European Centre for Medium-Range Weather Forecasts (ECMWF) re-analysis in Fig.2. The temporal (daily product) and spatial 1deg averaging around the site has been performed (except for MSI, where data for a given pixel or the average of two pixels (S-2A, S-2B), if available, is given). It follows that all instruments show the existence of ozone hole in early November and its disappearance in the last week of December, 2020. Data from all instruments closely follows all temporal oscillations of the TOC (see, e.g., the TOC wave centered at the day 45 (December 15) in Fig.2). There is temporal/ spatial mismatch between MSI/S-2 and other satellite measurements. In particular, the MSI/S-2 measurements provide the total ozone column on the spatial scale of 10m, which is not possible for other instruments (see Table 1). This could explain some differences seen in TOC derived from MSI as compared to other instruments.

Preprints (www.preprints.org) | NOT PEER-REVIEWED | Posted: 22 September 2021 doi:10.20944/preprints202109.0388.v1

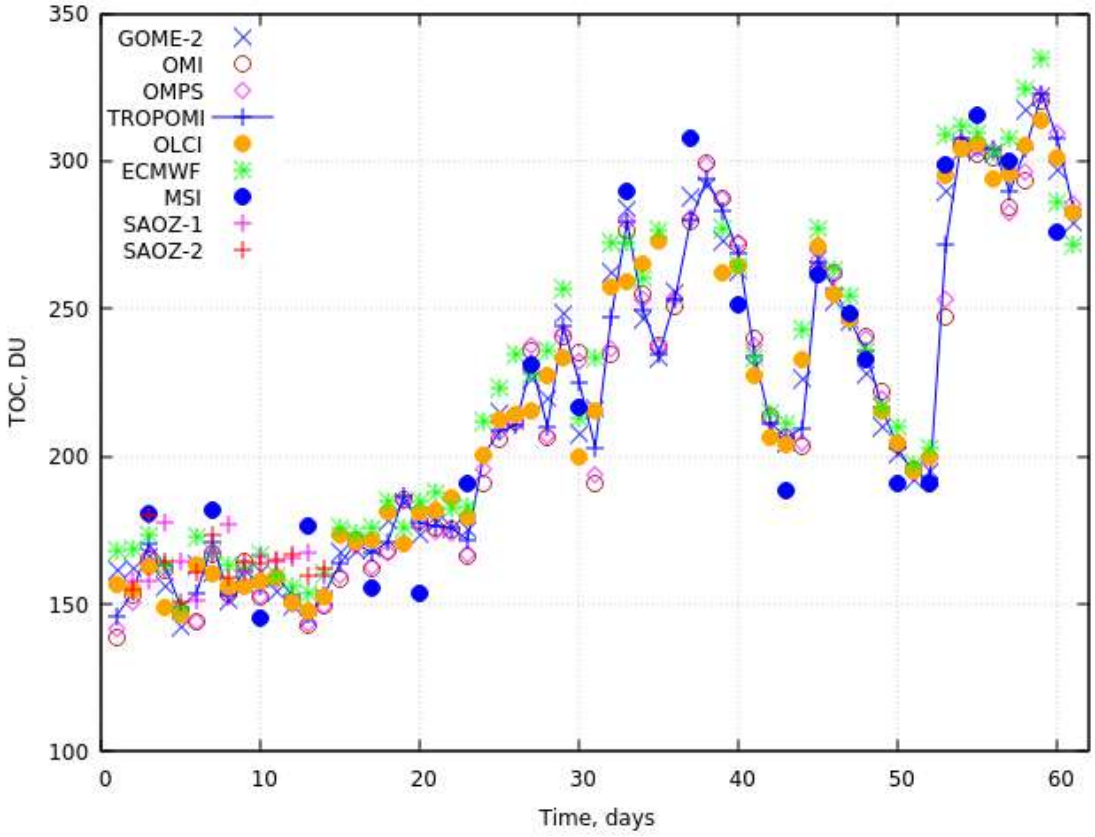

Fig.2. The total ozone column retrieved using MSI/S-2 observations and also other ground and satellite observations (see Table 3) at DOME C (Antarctica) on November-December 2020. The data derived from the ECMWF re-analysis is given as well.

Preprints (www.preprints.org) | NOT PEER-REVIEWED | Posted: 22 September 2021 doi:10.20944/preprints202109.0388.v1

Table 3. The instrumentation used in the determination of the total ozone column temporal changes over Dome C (Antarctica) shown in Fig.2. Further details on the satellite instrumentation used are given by Kokhanovsky et al. (2021b).

Instrument	Abbreviation	Spatial resolution
Global Ozone Monitoring Experiment	GOME-2	80×40km
Ozone Mapping and Profiling Suite	OMPS	$50 \times 50 km$
Ozone Monitoring Instrument	OMI	13×24km
TROPOsphere Monitoring Instrument	TROPOMI	7× 3.5km
Ocean and Land Colour Instrument	OLCI	0.3× 0.3km
MultiSpectral Imager	MSI	from 0.01× 0.01km till 0.06×0.06 km (dependent on the channel, see Table 1)
Système d'Analyse par Observations Zénithales (morning ground observations)	SAOZ-1	ground zenith sky transmittance measurements (morning)
Système d'Analyse par Observations Zénithales(evening ground observations)	SAOZ-2	ground zenith sky transmittance measurements (evening)

 doi:10.20944/preprints202109.0388.v1

The intercomparison of ground-based and satellite – retrieved albedo is given in Fig. 3 for December 9, 2016 (22:00:11UTC – ground measurements, 23:57UTC – satellite measurements, SZA= 65degrees). The ground measurements of the plane albedo have been performed in the spectral range 400-1050nm. Further details on the ground measurements are given by Picard et al. (2016b,c) and also by Kokhanovsky et al. (2019), where the same spectral albedo measurements have been used to validate the OLCI/S-3 snow albedo retrievals.

It follows that ground and satellite measurements of spectral albedo give very similar results, which indirectly confirm the validity of our assumptions used in the retrieval procedure. We also note that although we have used the spectral MSI/S-2 reflectance measurements at just two wavelengths (443 and 865nm), the spectral albedo is estimated in much larger spectral range useful also for the shortwave broadband albedo determination. This is due to the fact that the spectral pure plane snow albedo depends largely on two parameters – the effective absorption length and solar zenith angle. The difference between satellite and ground measurements depends on the wavelength being smaller than 2% in the spectral range 400-1100nm. This difference is below of the error of respective optical measurements. The largest differences (2%) occur around 1050nm, where MSI/S-2 does not perform any measurements. The ELAP estimated from the 864.7nm MSI-S2 channel may differ from that derived from 1020nm due to vertical snow inhomogeneity effects and spectrally dependant light penetration in snow layers. The difference observed in Fig.3a may be reduced if a new channel (say, 1020nm) is added to the MSI in the future.

Preprints (www.preprints.org) | NOT PEER-REVIEWED | Posted: 22 September 2021 doi:10.20944/preprints202109.0388.v1

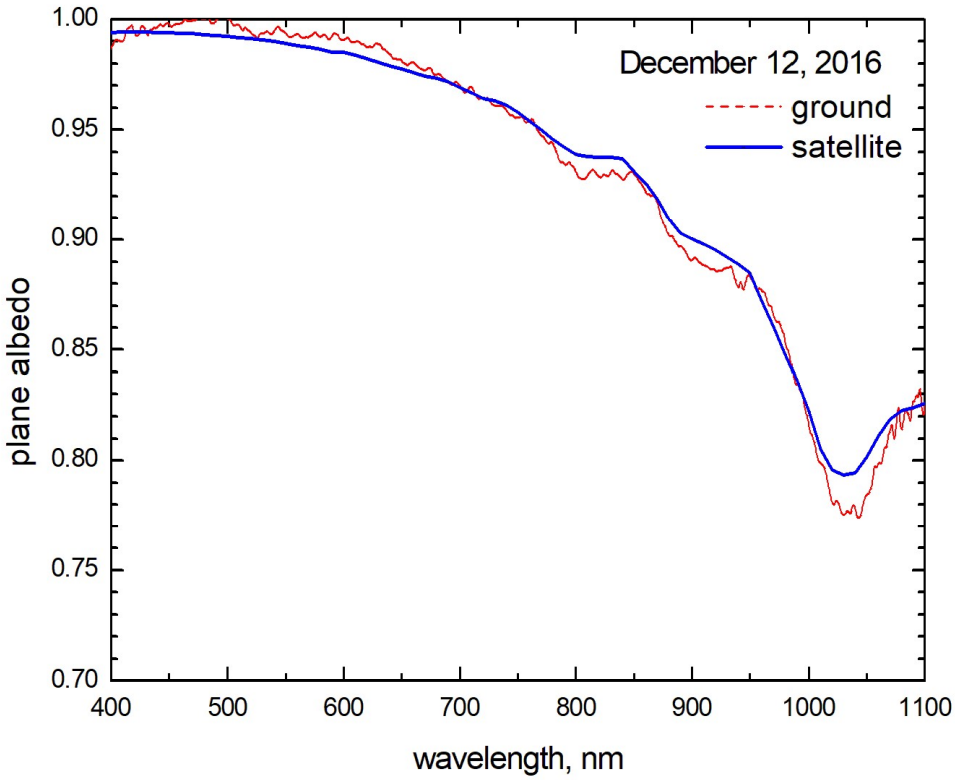

Fig.3a. The snow spectral plane albedo derived from dual – channel (443 and 865nm) satellite (blue line) and ground (red) measurements. The measurements have been performed on December 19, 2016 at Dome C in Antarctica. The satellite-derived snow albedo is provided on the spectral grid 10nm.

Preprints (www.preprints.org) | NOT PEER-REVIEWED | Posted: 22 September 2021 doi:10.20944/preprints202109.0388.v1

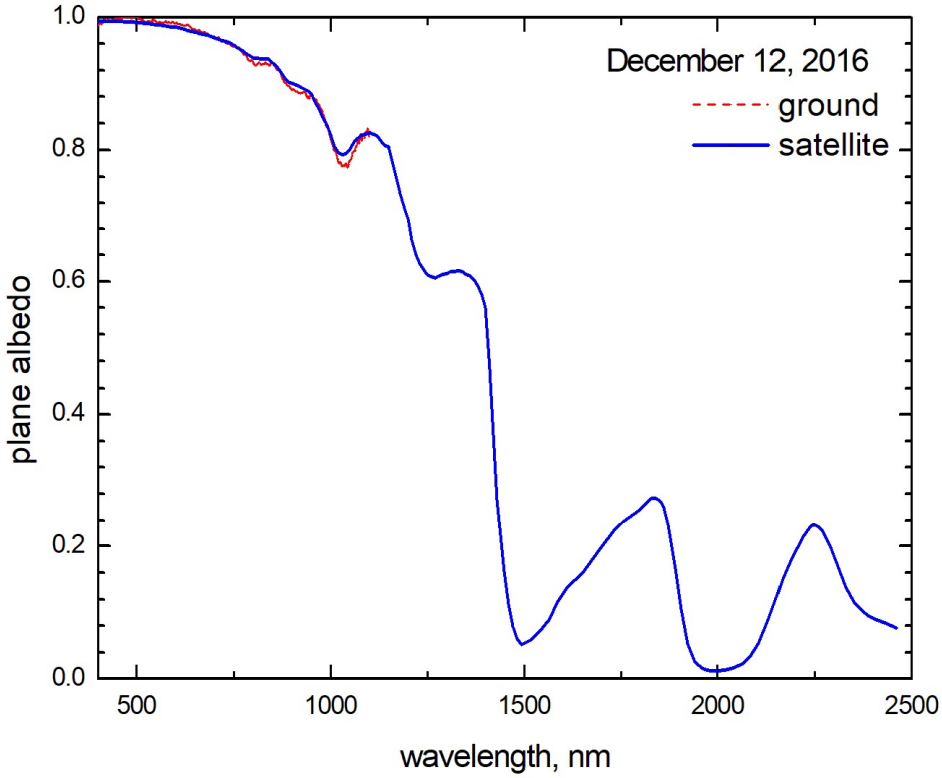

Fig.3b. The same as in Fig. 3a except for the larger spectral range.

3. Conclusions

We have proposed a simple algorithm to retrieve the total ozone column and snow properties (spectral albedo and effective light absorption path) using the high spatial resolution *single – view* MSI/S-2 measurements over Antarctica. Therefore, multiple observations of the same ground pixel from different directions as used, e.g., in the MODIS snow albedo retrieval algorithm (Schaaf et al., 2002) are not needed.

In addition, the algorithm allows the retrieval of the snow grain size on the scale 10 - 20m although this was not explicitly evaluated here. This algorithm should be useful for understanding of intra-pixel total ozone and snow albedo variability in complement to satellite

 doi:10.20944/preprints202109.0388.v1

observations performed on much coarser spatial resolution scale (0.3-1km and even larger spatial scales).

It has been shown that the MSI reflectance in the spectral range 443-865nm over snow in Antarctica can be modelled using just two parameters (K and L). These parameters are proportional to the total ozone column and the effective diameter of ice grains, respectively. Therefore, we conclude that the main parameters influencing the MSI spectra in the range 443-865nm are TOC and the effective diameter of snow grains with other effects of a secondary importance for a clean Antarctic atmosphere. In particular, the influence of the molecular and aerosol light scattering on the MSI/S-2 reflectance spectra in Antarctica can be neglected in the first approximation. This is especially true for the channel located at 865nm used for the effective grain diameter (see Eqs. (5)-(7)) and spectral albedo determination. We also assumed that the MSI reflectance at channel 1 (**8A**) is the same on the scale 10 and 60 (**20**)m, which is true for the most of Antarctic surfaces. Otherwise, the channels (2, 3, 8, see Table 1) having the same spatial resolution (10m) must be used to derive the pair (K, L) from Eq. (4). It follows from Fig.1 that the reflectances at channels 1 and 2 and also 8 and 8A have close values. Therefore, two different sets of channels used in the retrieval process produce almost the same retrieval results. Alternatively, the parameters (K, L) can be retrieved using all MSI channels in the framework of the optimal estimation approach.

The determination of the effective light absorption path makes it possible to estimate also snow broadband albedo (Kokhanovsky, 2021c) both from ground and satellite measurements.

Acknowledgements

The authors acknowledge the use of total ozone measurements performed by the SAOZ team (saoz.obs.uvsq.fr) and also derived using multiple ESA and NASA instruments (see Table 3) with many thanks. The authors thank ECMWF for providing forecasted TOC data.

References

Chen, N., Li, W., fan, Y., et al. (2021). Snow parameter retrieval (SPR) algorithm for GCOM-C/SGLI, *Rem. Sens. Env.*, in press.

Debella-Gilo, M., Gjertsen, A.K. (2021). Mapping seasonal agricultural land use types using deep learning on Sentinel-2 image time series. *Remote Sens.* 13, 289, https://doi.org/10.3390/rs13020289

Gascoin, S., Grizonnet, M., Bouchet, M., Salgues, G., and Hagolle, O. (2019). Theia snow collection: high-resolution operational snow cover maps from Sentinel-2 and Landsat-8 data. *Earth Syst. Sci. Data* 11, 493–514, https://doi.org/10.5194/essd-11-493-2019.

Gascoin, S., Barrou Dumont, Z., Deschamps - Berger, C., Marti, F., Salgues, G., López-Moreno, J.I., Revuelto, J., Michon, T., Schattan, P., Hagolle, O. (2020). Estimating fractional snow cover in open terrain from Sentinel-2 using the Normalized Difference Snow Index. *Remote Sens.* 12, 2904, https://doi.org/10.3390/rs12182904.

Gorelick, N., Hancher, M., Dixon, M., Ilyushchenko, S., Thau, D., Moore, R. (2017). Google Earth Engine: planetary-scale geospatial analysis for everyone, *Remote Sensing of Environment*, 202, 18-27, ISSN 0034-4257, https://doi.org/10.1016/j.rse.2017.06.031.

Flanner, M. G., Zender, C. S., Randerson, J. T., and Rasch, P. J. (2007). Present-day climate forcing and response from black carbon in snow. *J. Geophys. Res.*, 112, D11202, doi:10.1029/2006JD008003.

Flanner, M. G., Arnheim, J., Cook, J. M., Dang, C., He, C., Huang, X., Singh, D., Skiles, S. M., Whicker, C. A., and Zender, C. S. (2021). SNICAR-AD v3: A community tool for modeling spectral snow albedo, *Geosci. Model Dev. Discuss.* [preprint], https://doi.org/10.5194/gmd-2021-182, in review.

Free, G., Bresciani, M., Trodd, W., *et al.* (2020). Estimation of lake ecological quality from Sentinel-2 remote sensing imagery. *Hydrobiologia* 847**,** 1423–1438, https://doi.org/10.1007/s10750-020-04197-y

Gorshelev, V., Serdyuchenko, A., Weber, M., Chehade, W., and Burrows, J. P. (2014). High spectral resolution ozone absorption cross-sections – Part 1: Measurements, data analysis and comparison with previous measurements around 293 K. *Atmos. Meas. Tech*. 7, 609–624, https://doi.org/10.5194/amt-7-609-2014.

Grenfell, T. C., Warren, S. G., and Mullen, P. C. (1994). Reflection of solar radiation by the Antarctic snow surface at ultraviolet, visible, and near-infrared wavelengths. *J. Geophys. Res.* 99(D9), 18669– 18684, doi:10.1029/94JD01484.

Hall, D. K., Riggs, G. A., Salomonson, V.V., Di Girolamo, N. E., Bayr, K. J. (2002). MODIS snow-cover products, Remote Sensing of Environment, 83, 1–2, 181-194.

Iqbal, M., 1983: *An Introduction to Solar Radiation*, New York: Academic Press, p. 101.

Kang, S., Zhang, Y., Qian, Y., and Wang, H. (2020). A review of black carbon in snow and ice and its impact on the cryosphere. *Earth-Science Reviews* 210, 103346,ISSN 0012-8252, https://doi.org/10.1016/j.earscirev.2020.103346.

Kokhanovsky, A., Lamare, M., Danne, O., et al.(2019). Retrieval of snow properties from the Sentinel-3 Ocean and Land Colour Instrument. *Remote Sens. 11*, 2280. https://doi.org/10.3390/rs11192280.

Kokhanovsky, A. A., Lamare, M., Rozanov, V.V. (2020a). Retrieval of the total ozone over Antarctica using Sentinel-3 Ocean and Land Colour Instrument, *Journal of Quantitative Spectroscopy and Radiative Transfer* 251, 107045, https://doi.org/10.1016/j.jqsrt.2020.107045.

Kokhanovsky, A.A., Tomasi, C., Smirnov, A., et al. (2020b). Remote sensing of Arctic atmospheric aerosols, in *Physics and Chemistry of the Arctic Atmosphere* (ed. by A. Kokhanovsky and C. Tomasi, Springer Polar Sciences), 505-590, Cham: Springer.

Kokhanovsky, A., Box, J.E.,Vandecrux, B., Mankoff, K.D., Lamare, M., Smirnov, A., and Kern, M. (2020c). The determination of snow albedo from satellite measurements using fast atmospheric correction technique. *Remote Sens. 12*, 234. https://doi.org/10.3390/rs12020234.

Kokhanovsky, A., Di Mauro B., Garzonio, R., Colombo, R. (2021a). Retrieval of dust properties from spectral snow reflectance measurements. *Frontiers in Environmental Science* 9 , 42, https://www.frontiersin.org/article/10.3389/fenvs.2021.644551.

Kokhanovsky, A., Iodice, F., Lelli, L., et al. (2021b). Retrieval of total ozone column using high spatial resolution top-of-atmosphere measurements by OLCI/S-§ in the ozone Chappuis absorption bands over bright underlying surfaces, *J. Quant. Spectr. Rad. Transfer*, in press.

Kokhanovsky, A. (2021c). Snow broadband albedo, *Environmental Informatics and Remote Sensing, Frontiers in Environmental Science*, in press.

Mei, L., Rozanov, V., Pohl, C., Vountas, M., and Burrows, J. P. (2021a). The retrieval of snow properties from SLSTR Sentinel-3 – Part 1: Method description and sensitivity study, The Cryosphere, 15, 2757–2780, https://doi.org/10.5194/tc-15-2757-2021.

Mei, L., Rozanov, V., Jäkel, E., Cheng, X., Vountas, M., and Burrows, J. P. (2021b): The retrieval of snow properties from SLSTR Sentinel-3 – Part 2: Results and validation, The Cryosphere, 15, 2781–2802, https://doi.org/10.5194/tc-15-2781-2021.

Painter, T.H., Rittger, K., McKenzie, C., Slaughter, P., Davis, R. E., Dozier, J. (2009). Retrieval of subpixel snow covered area, grain size, and albedo from MODIS, *Remote Sensing of Environment*, 113, 4, 868-879.

Peng, X., Zhang, T., Frauenfeld, O. W., Du, R., Jin, H., Mu, C. (2021). A holistic assessment of 1979-2016 global cryospheric extent, *Earth's Future*, 9, e2020EF001969, https://doi.org/10.1029/2020EF001969.

Picard, G., Libois, Q., and Arnaud, L. (2016a). Refinement of the ice absorption spectrum in the visible using radiance profile measurements in Antarctic snow. *The Cryosphere* 10, 2655–2672, https://doi.org/10.5194/tc-10-2655-2016.

Picard, G., Libois, Q., Arnaudt, L., Vérin, G., and Dumont, M. (2016b). Development and calibration of an automatic spectral albedometer to estimate near-surface snow SSA time series. *The Cryosphere* 10(3), 1297-1316, https://doi.org/10.5194/tc-10-1297-2016.

Picard, G., Libois, Q., Arnaudt, L., Vérin, G., and Dumont, M. (2016c). Time-series of snow spectral albedo and superficial snow specific surface area at Dome C in Antarctica, 2012-2015. *PANGAEA*, https://doi.org/10.1594/PANGAEA.860945.

Pommereau, J.-P., Goutail, F. (1988). O3 and NO2 ground-based measurements by visible spectrometry during arctic winter and spring 1988. *Geophys. Res. Lett*. 15, 891–894.

Sarkissian, A., et al. (1997). Accuracy of measurements of total ozone by a SAOZ ground-based zenith sky visible spectrometer. *J. Geophysical Research* 102, 1, 1379-1390.

Savastiouk, V., McErloy, C. T. (2004). Calculating air mass factors for ozone and Rayleigh air mass factor calculations for ground – based spectrometers. Proc. Of Quadrennial Ozone Symposium,Kos, Greece, doi: 10.13140/2.1.3553.7284.

Schweizer, J., Kronholm, K., Jamieson, J. B., and Birkeland, K. W. (2008). Review of spatial variabilty of snowpack properties and its importance for avalanche formation, *Cold Reg. Sci. and Technology*, 51, 253 - 272.

Six, D., Fily, M., Blarel, L, Goloub, P. (2005). First aerosol optical thickness measurements at Dome C (east Antarctica), summer season 2003-2004. *Atmos. Env*. 39, 5041-5050.

Schaaf, C. B., Gao, F., Strahler, A. H., et al. (2002). First operational BRDF, albedo nadir reflectance products from MODIS, *Remote Sensing of Environment*, 83, 1–2, 135-148.

Tomasi, C., and Petkov, B. H. (2015). Specral calculations of Rayleigh – scattering optical depth at Arctic and Antarctic sites using a two – term algorithm, *J. Geophys. Res.* 10.1002/2015JD023575.

Wang, B., Jia, K., Liang, S., Xie, X., Wei, X., Zhao, X., Yao, Y., Zhang, X. (2018). Assessment of Sentinel-2 MSI spectral band reflectances for estimating fractional vegetation cover, *Remote Sens. 10*, 1927, https://doi.org/10.3390/rs10121927.

Warren, S., and Brand, R. E. (2008). Optical constants of ice from the ultraviolet to the microwave: a revised compilation. *J. Geophysical Research* 113, D14, https://doi.org/10.1029/2007JD009744.

Zhang, D., Fang, S., She, B., Zhang, H., Jin, N., Xia, H., Yang, Y., Ding, Y. (2019). Winter wheat mapping based on Sentinel-2 Data in heterogeneous planting conditions. *Remote Sens. 11*, 2647, https://doi.org/10.3390/rs11222647.